Wear 274–275 (2012) 414–422

Contents lists available at SciVerse ScienceDirect

Wear

journal homepage: www.elsevier.com/locate/wear

Improved ball crater micro-abrasion test based on a ball on three disk configuration

J.M. Fildes[a,*], S.J. Meyers[a], R. Kilaparti[b], E. Schlepp[c]

[a] Institute of Tribology and Coatings, 1019 Air Park Drive, Sugar Grove, IL 60554, USA
[b] College of Engineering and Engineering Technology, Northern Illinois University, 590 Garden Road, DeKalb, IL 60115, USA
[c] The Falex Corporation, 1020 Air Park Drive, Sugar Grove, IL 60554, USA

ARTICLE INFO

Article history:
Received 18 May 2010
Received in revised form 11 October 2011
Accepted 15 November 2011
Available online 25 November 2011

Keywords:
Three-body abrasion
Hardness
PVD coating
Steel
Wear testing

ABSTRACT

An improved ball crater micro-abrasion test method has been developed that differs from the conventional ball crater method. A ball-on-three-disk (BOTD) configuration provides mechanical stability and three simultaneous measurements of abrasion. An inclined BOTD geometry allows the specimens to be totally immersed in abrasive, which allows the use of dry abrasives as well as slurries and pastes. Use of a rubber ball gives effective three-body abrasion and provides results that are highly correlated with the ASTM G65 method. Use of dry abrasive with a rubber surface, rather than use of slurries and a metal ball, provides cutting action that is closer to actual field conditions, and allows high temperature test. Flooding the substrate with abrasive also avoids the problems encountered in conventional ball crater tests in that it provides spherical scars even for large particle abrasives, and spherical geometry allows direct computation of the volume of wear. Modeling of the BOTD scar geometry indicates that the BOTD contact pressure is similar to the contact pressures used in the ASTM G65 test. The BOTD microabrasion method provided excellent ranking of the abrasion rates of bare steel and two thicknesses of a TiAlN coating.

1. Introduction

Although abrasion is a process that involves cutting of a substrate by harder abrasive particles, there is much complexity because of the wide variety of abrasive particles, the different modes of material removal (plastic deformation leading to detachment of work hardened chips or fracture of low toughness materials) and different metal removal processes (plowing, wedge formation and cutting) [1]. Two-body abrasion, such as sandpaper, in which the abrasive particles are attached to a backing material, provides different abrasion rates and wear patterns than three body abrasion, in which the motion of the abrasive particles is not constrained. The hardness of the abrasive and the geometry of the abrasive particles also make substantial contributions to abrasion rates and wear patterns.

For the reasons just cited, many abrasive wear test methods have been developed. An example is the ASTM G65 method (Standard Test Method for Measuring Abrasion Using the Dry Sand/Rubber Wheel Apparatus), which involves dropping abrasive from a hopper into the contact zone of a rubber coated metal wheel and the test substrate. Although the ASTM G65 method is the most widely used method for assessing dry, three body abrasion; it is limited in which abrasives can be used by the need to achieve uniform flow of the abrasive through the feed nozzle of the hopper [2]. For example, fine dust and talc-like powders do not flow well and are difficult to use in the ASTM G65 method.

Less used abrasion test methods involve introducing abrasive particles into pin-on-disk and pin-on-drum tests, but these tests are usually limited to two-body abrasion or to abrasive slurries because the geometry and motion of these tests tends to move loose, dry abrasive particles out of the contact track. Another abrasion test, which is often referred to as a ball crater micro-abrasion test, involves using abrasive with a steel ball or wheel to make small craters in a test specimen [3]. Unfortunately, none of these test methods provides the ability to measure dry, three-body abrasion with the full variety of abrasives that are encountered in actual use. For example, a common need is to measure abrasive wear of dust particles trapped between two sliding surfaces, in which one of the surfaces is usually softer than the other. A rubber surface sliding against a hard disk is ideal to simulate this type of situation since the abrasive becomes embedded in the rubber surface, which protects the rubber surface from experiencing abrasive wear and which also more effectively drags the abrasive over the specimen in a way that provides more effective cutting action [4]. The rubber counter surface is also tough, which helps to avoid abrasion of the rubber. Although a rubber counter surface is provided by the ASTM

* Corresponding author. Tel.: +1 630 556 9700; fax: +1 630 556 9710.
E-mail address: jfildes@tribologyinstitute.org (J.M. Fildes).

0043-1648/$ – see front matter © 2011 Elsevier B.V. All rights reserved.
doi:10.1016/j.wear.2011.11.003

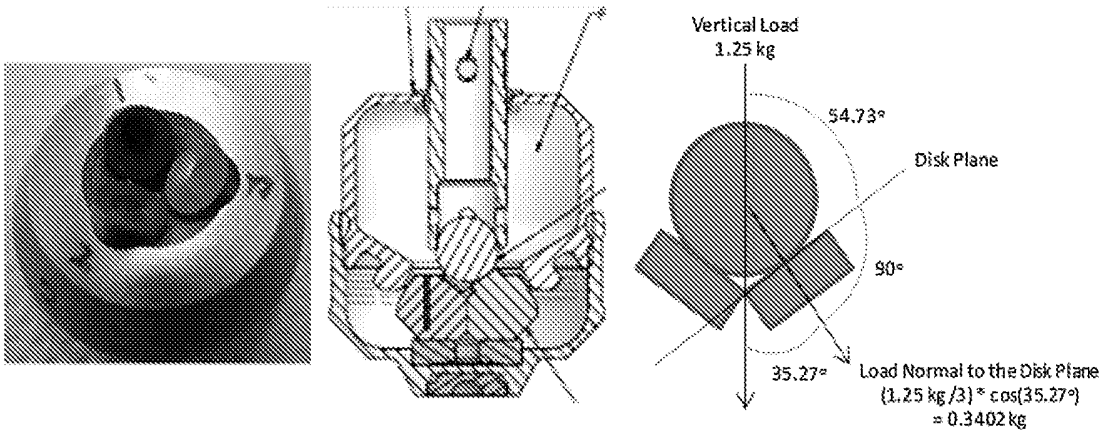

Fig. 1. BOTD specimen geometry.

G65 method, this method limits the types of abrasives that can be examined and the conventional ball-cratering micro-abrasion test requires the abrasive particles be in a slurry or paste.

The ball-on-three-disk (BOTD) test geometry has historically been used for evaluating the lubricity of fuels. This test involves sliding a metal or ceramic ball over three disks that are immersed in the fuel to be tested. The extent of wear that is observed on the disks is well correlated with the lubricity of the fuel [5]. Our work was motivated by recognition that replacement of the metal or ceramic ball with a rubber ball would provide an effective test for dry, three body abrasion that should provide similar results to the ASTM G65 method and that would have the advantage that the sample could be flooded with abrasive, or exposed to a dusting of particulate or blowing particulate. The BOTD also allows abrasion tests to be conducted with and without lubrication, and it allows use of slurries, elevated temperatures, controlled environmental conditions, and oscillatory and unidirectional motion.

2. Experimental

The geometry of the BOTD ball and specimens is shown in Fig. 1, in which only two of the three specimen disks are shown. We adapted a commercially available Falex BOTD for this study. The Falex design uses a trapped ball and provides for independent loading of the ball on the specimen disks. In the Falex BOTD, the line from the center of the ball to the center of each disk is at an angle of 35.27° from the vertical line along which the load is applied. A vertical load of 1.25 kgf was applied in our tests, which results in a loading by the ball of 0.340 kgf normal to each disk.

The modifications we made to the commercially available BOTD unit made by the Falex Corporation for testing the lubricity of fuels involved: (1) using a 1.27 cm diameter neoprene ball with a 70 Shore Adurometer, (2) flooding the sample chamber with 25 grams of sand of the same type that is used in the ASTM G65 test (AFS50/70), and (3) applying a load of 1.250 kg, which is one half the normal BOTD lubricity test load. We used the normal BOTD lubricity test rotational speed (60 rpm) with unidirectional rotational motion of the ball, which provides sliding motion of the ball on the substrate. The track of the ball in contact with the three pads has a diameter of about 0.73 cm, so 60 rpm produces a sliding speed of 0.023 m/s. A fresh 20 ml sample of sand was used for each test. The rather steep angle of the pads and the rotation of the ball cause significant stirring of the sand. This, coupled with the low contact stress, results in no fracturing or visible changes in the angularity of the sand particles as observed microscopically. The test duration was 3 h. We also measured the thickness of the coatings using two-body abrasion by employing a 1.27 cm alumina ball. The same load and rotational speed were used, but the test duration was 60 min.

We examined three different specimens. One specimen was bare 4140 steel, the second was 4140 coated with 2.3 μm of TiAlN (titanium aluminum nitride), and the third was 4140 coated with 4.1 μm of TiAlN. The hardness of TiAlN is 3400 Vickers, and the hardness of the heat treated 4140 is 34 R_C (about 335 HV). This evaluation therefore provides the ability to observe how the measured abrasion wear rates scale with hardness, since abrasion wear rates tend to correlate well with specimen hardness, as well as how abrasive wear rates scale with coating thickness.

Three disks are used in each BOTD trial. The three disks can either be the same material, which provides three replicates of the measured wear rate, or each of the three disks can be a different specimen material, which provides a direct comparison of the wear rates for each specimen for each BOTD trial. Each BOTD trial results in a wear scar on each of the three disks, and the profiles of these scars were measured by a Zeiss Model 1400A profilometer. The scars appear to be spherical, so we obtained a single profile trace through the apex of the scar. Our testing utilized three replicates of a given specimen material for each BOTD trial, and multiple trials were pre-formed to provide enough data for good quality statistical analysis. Parameters that characterize the measured scars, such as the width and depth, were obtained by graphical techniques and by least squares curve fitting using a custom routine in MathCAD 14.

3. Theory

The rotating ball on disk configuration, also called the ball crater micro-abrasion method, has most commonly been used to measure the thickness of coatings as shown in Fig. 2 [6]. In this case, abrasive slurry is used and the particle size influences the quality of the observed scar and the accuracy of the thickness measurement.

The coating thickness, t, is computed from the scar dimensions x and y identified in Fig. 2 and from the ball's radius, R:

$$t = \frac{x \times y}{2 \times R} \quad (1)$$

The rotating ball on disk configuration has also been used to measure the wear rate of coatings, but this is more challenging than measuring the wear rate of monolithic materials because coatings and substrates can have very different wear rates and the ideal test methodology would be to measure wear of the coating without causing breakthrough and comparing this to wear of the substrate for a similar period of time. In reality, wear tests of coatings are almost never done this way because it requires much trial and error

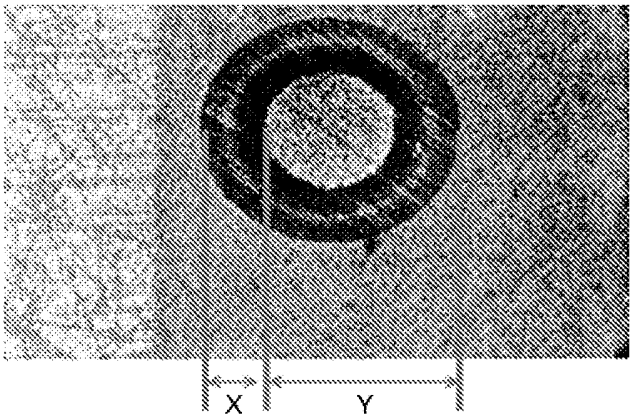

Fig. 2. Typical ball crater coating thickness measurement. (Modeled after Thompson, Ref. [10]; dimensions added.)

to determine how long the test can run without causing breakthrough of the coating, and many coatings, especially very hard ones, are very thin, which makes it difficult to stop the test before the coating breaks through. This difficulty is especially true for an aggressive test such as the ASTM G65 abrasive wear test.

In actual practice, wear testing of coatings typically subjects the coating and substrate to the wear process used in the test for a fixed time period, or for a fixed number of cycles, or fixed sliding distance. Although this test methodology is more practical, it usually causes breakthrough of the coating, which provides a wear rate that is a composite of that of the coating and of the substrate. In this case, the wear volume is the most direct measure of the extent of wear since it does not require any corrections for density differences of various materials [7]. Nonetheless, direct measurement of the wear scar volume may be difficult to achieve. For example, wear scars of coated substrates in the ASTM G65 test can show very irregular borders for which it is difficult to define a smooth contour for the wear scar, which is required to obtain an accurate scar volume. In contrast, a ball on disk configuration produces a well-defined scar geometry that makes it practical to directly obtain the wear volume.

In theory, a rigid spherical body spinning against a disk should produce a spherical wear scar and this is significant because it allows straightforward geometric calculations to be used to define the wear volume. This is accomplished by recognizing that the surface of the spherical wear scar defines a small circle of a sphere. A small circle of a sphere is the circle defined by any plane through the sphere that does not contain the center of the sphere, for example the circle defined by the plane $K'C'A'$ in Fig. 3. For simplicity of visualization, the circular cross section of the scar that occurs at the apex of the spherical scar can be considered, as is also shown in Fig. 3. The width of the scar is w, the depth is d, and the radius is r.

The observed depth, d, and width, w, of the wear scar can be measured with a microscope, or with aprofilometer, and the Pythagorean relationship shown in Fig. 3 can be solved for the radius, r, from the formula:

$$r = \frac{d}{2} + \frac{w^2}{8 \times d} \tag{2}$$

The scar radius and depth can be used to compute the scar volume, V, from the formula:

$$V = \Pi \times d^2 \times \left[r - \frac{d}{3} \right] \tag{3}$$

The volume could have been computed directly by substituting the equation for the radius into the equation for the volume, but it is valuable to compute the radius explicitly because the radius helps to explain the geometry of the scars as will be discussed below.

The BOTD ball can be made from any material, but use of rubber allows the ball on disk test to function in a way that should be similar to the well-established ASTM G65 abrasion test. As in the G65 test, the BOTD's rubber ball will become coated with abrasive particles, which protects the rubber ball from wear and which contributes to more effective dragging of the abrasive particle against the specimen disk. Although a single ball on disk is sufficient for the test, there are important advantages in a three ball on disk (BOTD) configuration. The obvious advantage is that each test produces three simultaneous measurements. Additionally, the BOTD arrangement allows the disks to be placed on an angle while better supporting the load and resisting vibrations. Placing the disks on an angle allows the BOTD to be designed such that the specimen holder can move and allow for self-centering of the ball, which ensures uniform loading of the three disks. Placing the disks on an angle is also important because it allows the specimen area to be flooded with abrasive, and it creates a continual flow of abrasive into the ball-disk contact zone. This is far superior, especially for abrasives that do not flow well, to dropping abrasive from a hopper as is done in the ASTM G65 test.

The BOTD offers other important advantages. These include: lubricants can be easily incorporated into the testing; oscillatory as well as unidirectional motion can be used; ceramic balls can be used for two body abrasion tests; slurries can be evaluated; the test specimens can be heated; and the ambient conditions, such as humidity, can be controlled.

4. Results

We measured the thickness of the TiAlN coatings used in this study both to confirm the nominal coating thicknesses that were provided by the fabricator and to provide a practical demonstration of the use of two-body abrasion in the BOTD test. The results are shown in Table 1. We conducted two BOTD trials with each coating thickness and three separate pads are examined in each trial, for a total of six measurements of each coating thickness. The thin specimen has an average thickness of 2.34 μm and the thick specimen has an average thickness of 4.11 μm.

The measured data for the BOTD abrasion test are the scar depth and scar width, and the results of our testing are shown in Table 2. Three disks of the same material composition are tested in each BOTD trial, which results in three replicate measurements of wear for each trial. The numbers shown for each trial in the top block of the table are the averages of the measurements for the three disks for each trial. The Grand Average is the average of the "trial averages." The second block in the Table shows the standard deviations divided by the corresponding average of the measurements, which simplifies interpretation of the standard deviations. The data for the width and depth of the wear scars of each set of three disks of each trial for 4140 steel and 4140 coated with 4.1 μm of TiAlN show good consistency, with standard deviations that are typically 10% or less of the average values. There is also good repeatability from trial to trial for 4140 and 4140 coated with 4.1 μm of TiAlN as is shown by the Grand Averages, which are about 10% for these two different specimens. The 2.3 μm TiAlN trials show much greater variability, but this was not due to the test method, but rather to the fact that the duration of the test was such that complete breakthrough of the 2.3 μm coating occurred in this timeframe, and small changes in the amount of breakthrough cause substantially different scar widths and depths because of the much higher wear rate for 4140 steel as compared to TiAlN.

These results demonstrate the difficulties that can be encountered in abrasion testing and in testing hard coatings. Abrasion tests

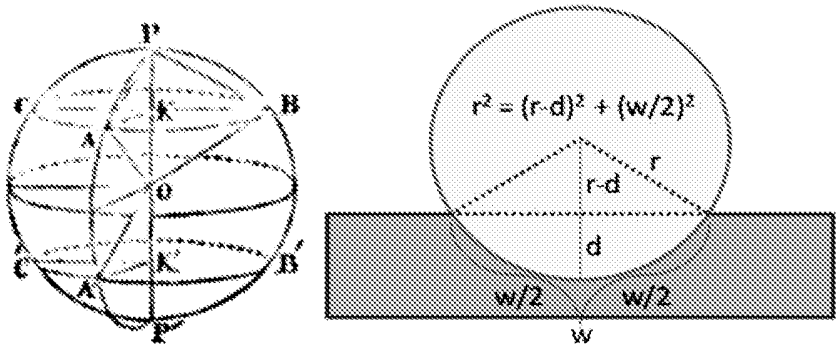

Fig. 3. Solid geometry of a spherical wear scar.

Table 1
TiAlN coating thickness.

ThinTiAlN Spcimen						ThickTiALN Specimen					
Outer diameter	Inner diameter	Outer radius (y), mm	Inner radius (x), mm	Ball radius, mm	Coating thickness, urn	Outer diameter	Inner diameter	Outer radius (y), mm	Inner radius (x), mm	Ball radius, mm	Coating thickness, urn
1.142	1.019	0.571	0.062		2.77	1.063	0.848	0.532	0.108		4.50
1.094	1.005	0.547	0.045		1.92	1.05	0.906	0.525	0.072		2.98
1.121	1.019	0.561	0.051		2.25	1.224	1.046	0.612	0.089		4.29
1.111	1.019	0.556	0.046	6.35	2.01	1.036	0.817	0.518	0.110	6.35	4.47
1.077	0.971	0.539	0.053		2.25	1.036	0.841	0.518	0.098		3.98
1.121	0.991	0.561	0.065		2.87	1.224	1.039	0.612	0.093		4.46
Average	1.004	0.556	0.054		2.34	1.1055	0.916167	0.553	0.095		4.11
Std. dev	0.020	0.011	0.0082		0.39	0.092	0.102	0.046	0.014		0.59

are inherently less consistent than other types of wear tests because of variation in the particle size and angularity of the abrasive and because the wear is caused by three body contact rather than two body contact. Measuring the wear of hard coating is challenging because of potentially widely different wear rates of the coating and substrate, as is the case in this study. Nonetheless, the degree of repeatability observed for the BOTD abrasion test is comparable with the repeatability of measured weight loss data observed for these specimen materials in the ASTM standard G65 abrasion test.

Also noteworthy, we examined the morphology of the sand contained within the BOTD specimen cup before and after the three-hour test period. For each test we used a fresh sample of sand (25 g). The rather steep angle of the pads and the rotation of the ball cause significant stirring of the sand. This, coupled with the low contact stress, results in no fracturing or visible changes in the angularity of the sand particles as observed microscopically. Likewise, the rubber ball did not exhibit any type of degradation. The wear scar formed on the pads also exhibited characteristics consistent with scratching. In fact, the vast majority of the scar, including the central portion, show fine scratches, while the very outer portion of the scar shows even finer scratches that are better characterized as polishing.

As was described in the Section 3, the scar width and depth shown in Table 2 allow the scar radius and volume to be graphically calculated. The results of the graphical calculation are shown in Table 3 along with the results from ASTM G65 abrasion tests for these same specimen materials.

The correlations between the various BOTD scar parameters and the ASTM G65 scar parameters are compiled in Table 4. The observed BOTD wear volumes correlate very well with the measured weight loss at 33.36 N applied load in the ASTM G65 test for these same materials, but not nearly as well with the ASTM G65 weight loss at 55.60 N applied load. It is difficult to directly measure the volume loss in the ASTM G65 test because the scar outlines are

Table 2
Measured scar depth and width for the BOTD abrasion test.

	2.3 μm TiAlN		4.1 μm TiAlN		Steel	
	Scar depth (mm)	Scar width (mm)	Scar depth (mm)	Scar width (mm)	Scar depth (mm)	Scar width (mm)
Trial			Values			
1	0.0220	1.8796	0.0058	2.9972	0.0754	4.1656
2	0.0154	2.2352	0.0047	3.2004	0.0800	4.1656
3	0.0187	2.1082	0.0049	2.5654	0.0614	3.7084
4	0.0116	1.9050				
Grand total	0.0169	2.0320	0.0051	2.9210	0.0723	4.0132
Trial			Standard deviations/Average value			
1	17%	10%	2%	5%	8%	1%
2	58%	12%	12%	4%	10%	3%
3	61%	15%	3%	9%	8%	2%
4	18%	18%				
Grand total	45%	14%	11%	11%	14%	6%

Table 3
Abrasive wear results with bare and coated 4140 substrates, neoprene counter surface, and G65 sand.

	BOTD scar Radius (mm)	BOTD scar Depth (mm)	BOTD scar Volume (mm)	G65 scar Depth (mm) at 33.36 N	G65 scar Depth (mm) at 55.60 N	G65 weight Loss (g) at 33.36 N	G65 weight Loss (g) at 55.60 N
2.3 (±0.4) μm TiAlN	43.18	0.01692	2.713E-11	0.02281	0.04958	8.5	49.0
4.1(±0.6) μm TiAlN	213.359	0.00514	1.746E-11	0.00465	0.00445	0.9	0.8
4140 Steel	27.94	0.07227	4.629E-10	0.05870	0.10676	34.0	86.5

rough, thus weight loss is a commonly used measure of the volume of material lost in the ASTM G65 test and it will correlate reasonably well to volume, although the correlation is not perfect since 4140 and TiAlN have different densities. It can also be seen from Table 4 that the BOTD scar depth correlates well with the G65 scar depth at 33.36 N applied load.

The accuracy of the BOTD and ASTM G65 wear indices can be assessed by comparing the relative amounts of wear of the two thicknesses of TiAlN to the ratio of their thicknesses. The ratio of the thicknesses is 0.57. The observed ratio of 0.64 for the BOTD scar volume is very close to the thickness ratio, whereas the ratio of 0.11 for the G65 result is not nearly as good of a match. The deviations of the observed results from the expected value are most likely due to the fact that breakthrough of the coatings was observed in all tests. Since wear after breakthrough of the coating is due to the wear of the much higher wear rate 4140 substrate, the observed wear volume ratio would be larger, and therefore even closer to the expected value, if breakthrough of the coatings did not occur. This is because the wear rate in the thinner coating test, which exhibits more breakthrough, would decrease more than the wear rate in the thicker coating test, which exhibits less breakthrough. Although the ideal is to have no breakthrough of the coating, this is impractical. Nonetheless, the BOTD test comes close to meeting the ideal situation and its scars show far less breakthrough than the ASTM G65 scars, which is why the BOTD result is much closer to the expected value, and also why the ASTM G65 test at 55.60 N produces a wear ratio that is even farther from the expected value than the ASTM G65 result at 33.36 N.

Abrasion wear resistance is roughly proportional to hardness and the BOTD and ASTM G65 wear volumes that were observed for 4140 and TiAlN follow this trend. Although there is likely not a one-to-one correspondence between the reciprocal of the hardness and the observed abrasion rate, this ratio does provide an approximate comparison. A relative abrasion rate of 0.099 for TiAlN as compared to 4140 steel would be expected based on a one to one correspondence of the ratio of the reciprocal of the hardness values of these two materials (3400 Vickers for TiAlN and 335 Vickers for4140). The observed ratio for 4.1 μm TiAlN, which provides the least coating breakthrough in these tests, and 4140 steel is 0.04 for the BOTD scar volumes and 0.03 for the G65 weight loss at 33.36 N applied load. The somewhat smaller ratios than were expected are at least partly due to the fact that substantial breakthrough did occur in each test.

5. Discussion

Ball crater measurements of coating thickness use abrasive slurry to form the scar, and there is literature that indicates that the size of the particles in the slurry affect the quality of the scar and of the thickness determination [8]. In contrast, we improved on the common technique by using two-body abrasion with an alumina ball, which removes particle size from having an influence on the outcome. Control of the surface finish of the alumina ball is much better than of the spread of particle size in slurry, and variability of abrasion is much less for two-body abrasion than for three-body abrasion with a slurry.

Our measured thickness results indicate an important aspect of PVD coatings. The thickness of PVD coatings is dependent on where the substrate is in the reactor, and fabricators usually specify a range of 1–2 μm for coating thickness because of this. The fabricator of the coatings used in this study specified them as 2.5 μm and 5 μm, whereas they are actually 2.34 μm and 4.11 μm. We believe the observed range of thickness values in Table 1 is more related to actual variation of coating thickness than to the test method, which indicates that 95% (two standard deviation units) of the specimens we tested should lie between 1.56 μm and 3.12 μm for the thinner coating, and between 2.93 μm and 5.29 μm for the thicker coating.

It is valuable to compare the BOTD average contact stresses to those in the ASTM G65 test. The geometries of the two tests are shown in Fig. 4, although the contacts in each test do not lie in a horizontal plane as is shown here for simplicity. Sand is dropped onto one side of the cylinder-substrate contact in the G65 test so a cylinder on flat plate model is appropriate, but the computation for the BOTD is more complicated because the BOTD is flooded with sand and the ball has a relatively small diameter so sand is likely part of the contact geometry in the BOTD test. A ball in a spherical socket model was used for the BOTD. For the ASTM G65 experiments, the rubber wheel was 22.8 cm in diameter, the length of contact with the plate was 1.27 cm, and the load holding the wheel against the plate was either 33.36 N or 55.60 N. The BOTD test parameters are given in the Section 2.

The modulus of elasticity of rubber is 0.1 GPa and the Poisson ratio for rubber is 0.5. The modulus of elasticity for TiAlN is 600 GPa, and Poisson's ratio is 0.25. We used Roark's formulas for a cylinder on a flat plate and for a ball in a spherical socket to compute the contact areas and maximum contact stresses [9]. These formulas are based on Hertz's theory. The calculation for the cylinder on a flat plate is straightforward, but the calculation for the ball in a spherical socket contains the radius of the spherical socket, the value of which is not known exactly because sand is a loose medium.

Our strategy to determine the radius of the socket was to set the value of the radius of the spherical socket to that which provided a contact diameter equal to the observed scar width for an actual BOTD wear scar that has a minimal depth of penetration. Minimal depth of penetration is important because the scar radius increases as the scar depth increases simply because more of the ball penetrates the flat plate, whereas we need the scar diameter that results prior to substantial penetration of the ball into the flat

Table 4
Correlation between BOTD and ASTM G65 data.

	BOTD scar Depth	BOTD scar Volume	G65 scar Depth at 33.36 N	G65 scar Depth at 55.60 N	G65 weight Loss at 33.36 N	G65 weight Loss at 55.60 N
BOTD scar radius	0.48	0.34	0.65	0.76	0.54	0.87
BOTD scar depth	1.00	0.98	0.97	0.92	1.00	0.83
BOTD scar volume	0.98	1.00	0.90	0.82	0.96	0.70

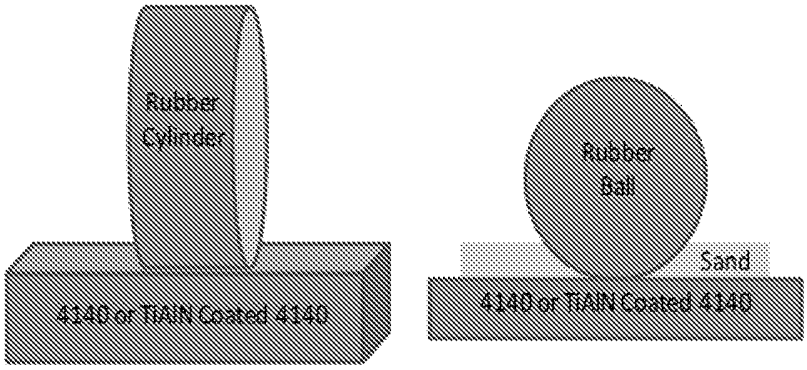

Fig. 4. ASTM G65 and BOTD abrasion tests.

plate. The scars we observed for the 4.1 μm TiAlN coating come closest to meeting this criterion because this coating is very hard and showed the least wear and the minimum scar depth in our tests.

Using the parameters given above for rubber and TiAlN coated 4140, a socket diameter of 1.32 cm gave a contact diameter that corresponded to the observed scar width (0.29 cm) for the 4.1 μm TiAlN coating. This socket diameter is slightly greater than the diameter of the ball (1.27 cm), so this seems like a reasonable result for loosely packed sand. The computed maximum contact stresses for the ASTM G65 are shown below (Table 5).

The three-body abrasion contact between the neoprene ball and uncoated 4140 was also modeled using the same approach of adjusting the socket radius to produce the observed scar width. In this case, the observed scar width was 0.401 cm, and the area was 0.1264 cm^2. A socket radius of 1.2890 cm reproduced the observed scar width and indicated a contact stress of 4.0 kgf/cm^2. The average depth of the uncoated 4140 scars is 0.0722 mm, whereas the average depth of the 4.1 μm TiAlN coated scars is 0.0051 mm. The socket radius would be expected to decrease as the scar depth increases as was observed because the scar the ball carves in the substrate has a tighter fit to the ball than does the loosely packed sand. The inverse relationship between the socket radius and the depth of the scar can be used to gauge what the contact stress may be at the beginning of the test. For example, a socket radius of 1.34 cm would correspond to a contact stress of 9.91 kgf/cm^2. This analysis also shows that although the BOTD abrasion test is not inherently a constant pressure test, it is effectively one because of sand forming a socket that carries some of the load of the ball and dramatically reduces the contact stress.

As described above, there is a very high correlation between the BOTD results and the ASTM G65 results for 33.36 N applied load and far less correlation for the ASTM G65 results at 55.60 N applied load, which is consistent with the computed maximum contact stress for the BOTD experiment, which is closest to that for the G65 test at 33.36 N. The result may be even closer because the BOTD scar we used to determine the socket radius is likely somewhat too wide due to penetration of the ball into the flat plate, and the average contact pressure increases as the socket radius decreases. The socket radius would ideally be computed from the scar at the earliest time at which the scar is clearly defined because the ball will have minimal penetration into the flat plate at this point. For example, a scar width of 0.254 cm (as opposed to the value of 0.289 cm that we used) corresponding to a socket radius of 1.348 cm (as opposed to the value of 1.32 cm that we used), would give a maximum contact stress of 10.05 kgf/cm^2, which is the maximum contact stress for the G65 test at 33.36 N applied load.

Table 5
Comparison of ASTM G65 and BOTD test conditions.

Test	Contact area (mm^2)	Contact stress (MPa)
G65 at 33.36 N load	43.225	0.772
G65 at 55.60 N load	56.128	0.991
BOTD at 3.34 N per pad load	6.129	0.545

These results indicate that the BOTD "flooded sand" abrasion test with a 12.23 N applied load approximates the maximum contact stresses of the ASTM G65 test at 33.36 N applied load, and therefore the BOTD test should provide similar cutting action and wear rates, which is in agreement with the strong correlation between our BOTD results and our G65 results for 33.36 N applied load and lack of strong correlation at 55.60 N applied load.

An assumption that was made in the BOTD test is that the BOTD scars are spherical since this allows easy and well-established equations to be used for computing the scar radius and volume from the scar's profile. Spherical scars are often observed in conventional ball cratering tests using abrasive slurries with small particles, typically 4–50 μm, but significant deviation from spherical shape is observed when using slurries with large particles such as the 212–300 μm range of the AFS50/70 sand that we used in our testing [6]. Non-spherical scars are also observed even for small particles in conventional ball crater test with dry abrasive [11]. In contrast, the scars in the BOTD tests appear to be spherical even for large particles since we used the same type of sand as was used in Ref. [6]. According to Ref. [6], use of large particles in the slurry of the conventional ball-cratering micro-abrasion test causes elongation of the scar in the direction of the spin of the ball. Use of larger abrasive particles in bench-scale testing is desirable because the larger particles are often encountered in actual field conditions.

Spherical wear scars are a significant advantage. As described in the Section 3 of this paper, spherical wear scars allow simple geometry to be used to directly compute the wear volume, whereas the loss of spherical geometry when using large particles in the conventional ball crater micro-abrasion test forced the researchers to use the indirect measure of mass loss in the work reported in Ref. [6]. Another advantage of the BOTD tests is that the rubber ball showed no degradation during 3 h test periods, whereas according to Ref. [6], the metal ball shows increasing surface roughness in the conventional ball-cratering micro-abrasion test and this increase in roughness alters the observed abrasive wear rate.

Although the observed BOTD scars appear to be spherical, this can be firmly established by fitting the (x,y) pairs of the scar profiles, where x is measured along the scar's width and y is the depth of the scar, to the equation for a circle in the form of:

$$y = y_0 + \sqrt{r^2 - (x - x_0)^2} \tag{4}$$

The parameters x_0 and y_0 are needed because the scar profile (x,y) pairs are measured in an arbitrary coordinate system so x_0 and y_0 are the center of the circle that defines the scar's profile,

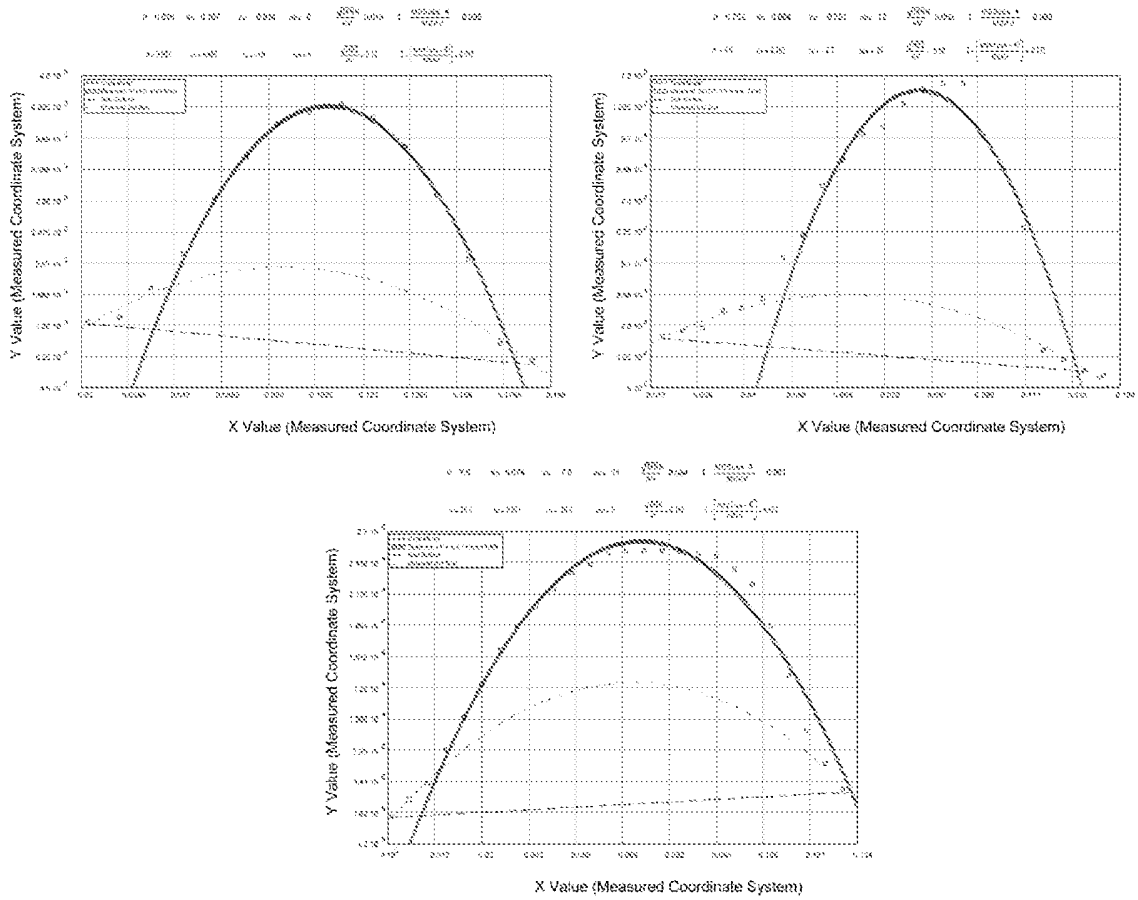

Fig. 5. Typical BOTD scar profile (4140 steel–left, 2.3 μm TiAlN–middle, 4.1 μm TiAlN–right).

and r is the radius of the circle. These parameters are adjusted by non-linear least squares techniques to minimize the mean squared error of the differences between the observed and calculated y values. This approach truly meets the assumptions underlying least squares since least squares techniques assume that all of the uncertainty is in the y values. The x (width direction) profile values are controlled by a stepper motor and are far more precisely known than the y (depth) values of the profile.

We examined 30 scars and typical results for 4140 steel and TiAlN coated 4140 steel are shown in Fig. 5. The non-linear least squares analysis results demonstrate that the observed scars are actually two scars, both of which are spherical. The outer scar likely arises from scuffing as opposed to cutting of the substrate that occurs in the region of the central scar. The asymmetry and displacement of the outer scar relative to the central scar is due to the incline of the test specimen. The centrifugal force of the spinning ball tries to propel sand away from the ball in the region of the outer scar. Gravity and the component of force applied to the ball that lies parallel to the disk's surface causes packing of the sand at the bottom of the disk as compared to the top of the disk (refer to Fig. 1), and this causes the observed scar profiles of the outer scars to show more wear at the bottom of the disk (at the left of the plots in Fig. 5) than at the top of the disk. In any case, the central scars are much larger than the outer scars and contain most of the wear volume so the outer scars can be ignored without causing much error in the computed wear volume. The excellent statistics of the least squares fits for the larger central scars confirm the fact that the scars are spherical. A quantity called R^2 provides an indication of the quality of the fit. R^2 is the ratio of the sum of the squares of the difference between the observed and calculated y values and the sum of the squares of the difference between the observed y values and the average of the y values. R^2 ranges from zero for no correlation to one for perfect correlation. The observed R^2 values were almost always larger than 0.90, and were often 0.98–0.99.

We also examined the correlation between the scar width, depth, and volume values that were obtained graphically and those that were obtained through the non-linear least squares analysis, and there is a greater than 0.99 R^2 value for the correlation between each of the corresponding parameters. This indicates that the far easier to perform graphical determination of the scar width, depth, and volume produces negligible error as compared to the more rigorous least squares technique.

The larger central scar profiles in Fig. 5 are significant to explaining the mechanism of formation of the scars. Table 3 shows that the large central scars have radii that range from 2.794 cm to 21.336 cm, which is substantially larger than the ball's radius of 0.635 cm and the scar radii are inversely proportional to the depths of the scars. In contrast, scar radii that are approximately equal to the radius of the ball are observed in BOTD tests with two body abrasion using an alumina ball and in adhesive wear tests using a steel ball, which indicates that the large BOTD abrasion test scar radii are related to the use of dry abrasive. Also, wear scars in conventional ball cratering micro-abrasion tests with small particle (4–50 μm) slurries have radii that are only about 6% larger than the radius of the ball, which indicates that the scar formation process for dry abrasive is different than for abrasive slurry [12].

We have used the ball in socket model Hertz contact deformation model described above in Fig. 4 to probe how the fundamental parameters, the width and depth, of the scar's geometry vary with scar depth for materials of different hardness. For a sequence of scar

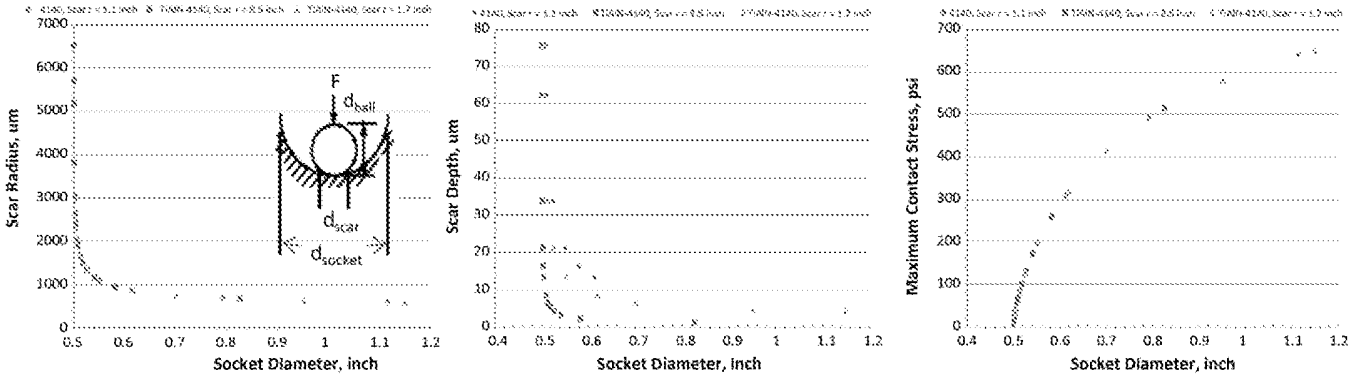

Fig. 6. Ball in socket scar model. (Left – scar radii, center – scar depth, right – contact stress vs. socket diameter.)

depths that cover the range that was observed in the BOTD abrasion test, Eqs. (3) and (4) were used with the observed average scar radii from Table 3 for 4140 steel (R = 2.794 cm), 2.3 μm TiAlN on 4140 (R = 4.318 cm), and 4.1 TiAlN on 4140 (R = 21.336 cm) to generate a table of values for each of the scar depth, scar radii, and scar volume values of the three specimens. The appropriate material parameters listed above for the three specimens were then inserted into the ball in socket model, and the socket diameter was used as an adjustable parameter to make the computed contact radius of the model match the scar radius at the depth values for each of the three materials as shown in the insert of Fig. 6. The socket diameter is a measure of the extent of wear. The diameter is initially defined by the loosely packed sand at the start of the test and is relatively large. The 4.1 μm TiAlN-4140 sample has the least wear (shallowest scar) and most closely matches this case. Over the course of the test, as the scar develops, the socket is increasingly defined by the scar and the socket diameter declines. The bare 4140 sample has the deepest scar and the 2.3 μm TiAlN-4141 sample has an intermediate scar depth.

Fig. 6 shows the relationship between scar radii (or width) and the socket diameter for each material and the three curves lay exactly on top of each other, which indicates that the scar formation mechanics are set by the test itself and are independent of the hardness (or alternatively the wear resistance) of the specimen and of the depth of the scar. In contrast, the scar depth curves do not lie on top of each other for depths below 30–40 μm. These two observations indicate that for any given scar width, or corresponding socket diameter, changes in the wear rate of the samples are only reflected by the depth of the scar, which also means that the effective radius of the scars are different as was observed.

There are two factors that could determine if the observed scars are spherical and why the radius would vary as is observed. One factor is variation of the pressure between the abrasive and the test specimen, which can be computed by trigonometric means as a function of position on the ball. The force applied on the ball is normal to the substrate only at the center of the contact between the ball and substrate, and the applied force splits into vertical and horizontal components when one moves away from the center of the contact between the ball and the specimen. Outside of the contact zone between the ball and the substrate, the vertical component is the force that pushes abrasive against the substrate. The second factor is that abrasion likely occurs beyond the contact zone (between the ball and test specimen) because of abrasive particles being moved by the ball and subsequently moving other particles. The ball's effectiveness in moving abrasive particles outside of the contact zone with the substrate in a way that cuts the test

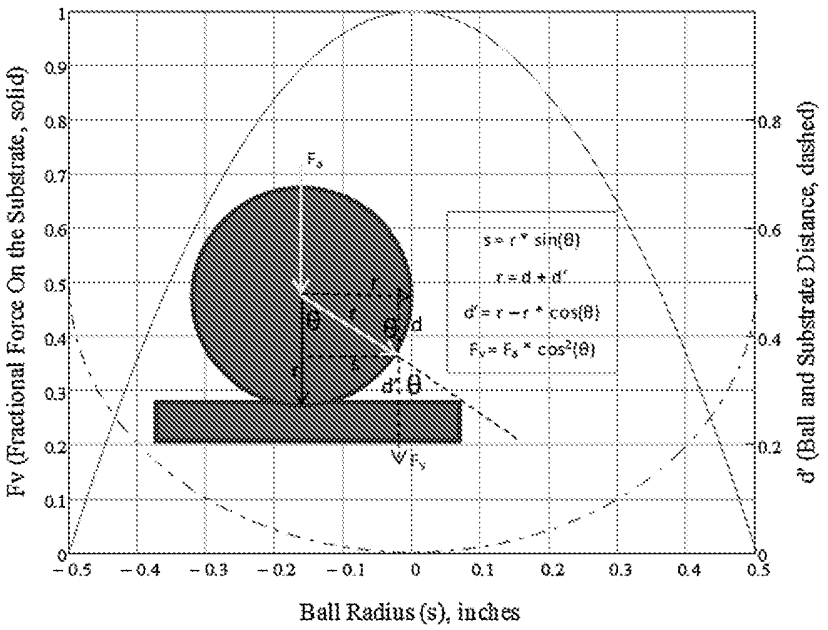

Fig. 7. Variation of the force (solid curve) and distance (dotted curve) between the ball and test specimen.

specimen will be related to the number of layers of abrasive between the ball and the test specimen, and this will depend on the separation between the ball and test specimen, which can also be computed by trigonometric means.

The results of the two computations described in the last paragraph are shown in Fig. 7, from which it is clearly seen that the force pressing the particles against the substrate varies in a parabolic manner as the square of the cosine of the angle between the direction of applied force and the vector to various spots on the ball's surface, whereas the spacing between the ball and substrate, which is related to the number of layers of sand, varies in a spherical manner as the cosine of the same angle. The fact that the observed wear scars have a spherical shape indicates that the reduction in the effectiveness of the cutting action as the number of layers of particles (i.e. the distance) between the ball and the substrate increases is the dominant mechanism in determining the profile of the scars.

This explains why the radii of the scars are larger than the radius of the ball since the ball can move several layers of sand, and this allows the cutting action on the substrate to occur with decreasing effectiveness for some distance from the point of contact between the ball and substrate, which produces radii that are larger than the radius of the ball. This also explains why harder materials produce the largest radii because it indicates that there are two wear rates that define the scar's shape. The larger wear rate is for the central portion of the scar in which direct contact occurs between the ball and the substrate and the other, smaller wear rate, is for the outer portion of the scar where the ball is moving several layers of sand to cause abrasion. Very hard, wear resistant coatings reduce and equalize these wear rates and result in larger radii scars. Softer materials allow the two different wear rates to be more fully manifested and result in scars with smaller radii, which reach a limiting value for deep penetration of the ball into the substrate that causes the scar to be fully defined by contact with the ball. The analysis in Fig. 6 clearly shows the merging of the scar curves as the depth reaches about 30 μm.

The maximum contact stress curves are also in Fig. 6, from which it is seen that the maximum contact stress curves also lay on top of each other for each material. The maximum contact stresses are low, starting under 1000 psi at the beginning of the test and ending at about a few tens of psi at the end of the test. Although the contact stresses change during the test, the low values indicate that the BOTD test can be considered a constant pressure test as far as wear is concerned because studies have shown that abrasive wear rates are independent of contact stress when the stresses are low [13]. In addition, the BOTD contact stresses do not cover a wide range.

6. Conclusions

The BOTD geometry provides a highly controlled (with respect to test parameters and ambient conditions), extremely flexible, robust, relatively simple, and easy to use test method and instrument that provides very consistent and meaningful results for measuring abrasion resistance. This study examined a relatively soft substrate and two thicknesses of a coating that has about the highest hardness as is currently available, and the BOTD abrasion test results provide excellent differentiation of these three specimens, which is a challenging task. The BOTD maximum contact stress can be adjusted to match the maximum contact stresses that are commonly used in the ASTM G65 test and the use of a rubber ball in the BOTD test causes the abrasive to be dragged across the substrate in the same way that occurs in the ASTM G65 test, all of which produces excellent correlation between the two tests. The BOTD produces better-defined scars than the ASTM G65 method and the BOTD scars are spherical, which allows direct graphical determination of the BOTD scar volume. The BOTD allows use of dry abrasives or slurries of small or large particles while still producing spherical scars, which is superior to conventional ball-cratering micro-abrasion tests.

Acknowledgement

The authors gratefully acknowledge the support of the U.S. Army's Benét Laboratories. Portions of the work discussed in this paper were funded by a U.S. Army contract.

References

[1] R. Chattopadhyay, Surface Wear, Analysis, Treatment and Prevention, ASM International, Materials Park, OH, 2001.
[2] K. Budinski, Guide to Friction, Wear and Erosion Testing, ASTM International, West Conshohocken, PA, 2007.
[3] B. Bhushan (Ed.), Modern Tribology Handbook, CRC Press, Boca Raton, 2001.
[4] M.J. Heale, M. Gee, Guide to Wear Problems and Testing for Industry, William Andrew Publishing, Norwich, NY, 2001.
[5] A. Wilcox, C.D. Gray, G.D. Webster, P.St. Pierre, K. Mitchell, D. Sporleder, Investigation of diesel fuel lubricity and evaluation of bench tests to correlate with medium- and heavy-duty diesel fuel injection equipment component wear – Part 1 SAE Document Number: 2002-01-1700, SAE International, Warrendale, PA, 2002.
[6] G.B. Stachowiak, G.W. Stachowiak, J.M. Brandt, Ball-cratering abrasion tests with large abrasive particles, Tribiol. Int. 39 (2006) 1–11.
[7] D.M. Kennedy, M.S.J. Hashmi, Methods of wear testing for advanced surface coatings and bulk materials, J. Mater. Process. Technol. 77 (1998) 246–253.
[8] Finer particle size allows better coating characterization with the Calotest, CSM Instruments Application Bulletin 5, October 1997.
[9] Bodies under direct bearing and shear stress, Table 33-Formulas for stress and strain due to pressure on or between elastic bodies, in: W.C. Young (Ed.), MathCAD CD ROM Electronic Book Adaptation of Roark's Formulas for Stress and Strain, 6th ed., McGraw Hill, MathSoft, Cambridge, MA, 2005, chapter 13.
[10] V. Thompson, H.E. Hintermann, L. Chollet, The determination of composition depth profiles using spherical erosion and scanning auger electron spectroscopy, Surf. Technol. 8 (1979) 421–428.
[11] D.N. Allsopp, I.M. Hutchings, Micro-scale abrasion and scratch response of PVD coatings at elevated temperatures, Wear 251 (2001) 1308–1314.
[12] C. Leroy, K.I. Schiffmann, K. van Acker, J. von Stebut, Ball cratering and efficient tool for 3 body microabrasion of coated systems, Surf. Coat. Technol. 200 (2005) 153–156.
[13] R.A. Erck, O.O. Ajayi, Analysis of sliding wear rate variation with nominal contact pressure, in: International Joint Tribology Conference, San Francisco, October 22–24, 2001.